

**Experimental study of Raman-active two-level systems in soda-lime-silica and lead oxide glasses**

J. J. Tu and A. J. Sievers

*Laboratory of Atomic and Solid State Physics and Cornell Center for Materials Research, Cornell University, Ithaca, New York 14853-2501*

(Received 6 August 2001; revised manuscript received 26 November 2001; published 29 March 2002)

An experimental study of the low-frequency, low-temperature Raman scattering from two-level systems (TLS) has been carried out for a series of soda-lime-silica glasses with various amounts of CaO and BaO and also for a Steuben (PbO) glass. Raman scattering from the resonant interaction with TLS is observed for both kinds of glasses. Because of the experimental precision of these measurements, it has been possible to estimate the Raman-active TLS number density and to show that it does not scale with the strength of the boson peak in the vibrational spectrum. The cutoff in the Raman activity of TLS for all of these glasses is consistent with earlier far-infrared absorption studies.

DOI: 10.1103/PhysRevB.65.144204

PACS number(s): 63.50.+x, 78.30.-j, 78.30.Ly

**I. INTRODUCTION**

A quasielastic component in the light scattering spectrum of a glass was first discovered in fused SiO<sub>2</sub> in 1975.<sup>1</sup> The increase in the low-frequency Raman scattering with increasing temperature was attributed to the scattering due to relaxation of two-level systems (TLS) between two possible configurations.<sup>2</sup> It was pointed out in this study<sup>1</sup> that the direct coupling of the light to the distribution of TLS should give rise to a characteristic temperature dependence associated with the thermal population of the two levels, but no such temperature dependence was seen. At about the same time temperature-dependent far-infrared absorption measurements demonstrated that the TLS energy distribution in glasses extended at least up to a frequency of 10 cm<sup>-1</sup>.<sup>3,4</sup> The predicted temperature-dependent properties of the low-frequency Raman scattering from resonant interactions with TLS was thought to have a firm theoretical footing,<sup>2</sup> but it became evident with the precise and systematic studies of the low-frequency and low-temperature Raman scattering in very pure silica fibers<sup>5,6</sup> that this spectroscopic probe could not identify TLS in vitreous silica. These experiments failed to show any evidence of the predicted hallmark temperature dependence associated with the resonant interaction with TLS. The missing signature was quite surprising since by this time the low-frequency end of the TLS density of states had been observed using many different experimental probes.<sup>7,8</sup>

This Raman inactivity issue reappeared over a decade later when it was experimentally demonstrated by both far-infrared absorption<sup>9,10</sup> and Raman resonant scattering<sup>11-13</sup> that a broad distribution of TLS existed in fluorite mixed crystals containing lanthanum. In addition, it was shown recently that the total Raman-active TLS number density can be estimated in these fluorite mixed crystals by using the allowed  $T_{2g}$  phonon mode as the normalizing factor.<sup>13</sup> These findings are of general interest since Raman scattering from resonant interactions with TLS has been observed in the oxide glass LASF7, which contains lanthanum.<sup>14</sup> Later these same investigators reported Raman scattering from TLS for a (NbTa) oxide glass, but not for a lead silicate glass even though the latter is also an efficient Raman vibrational

scatterer.<sup>15</sup> The total Raman-active TLS number density was not estimated for these systems. The fact that TLS are identified by Raman scattering in some glassy hosts but not in others is the current situation.

A fairly universal Raman feature in the low-frequency spectrum ( $<150$  cm<sup>-1</sup>) of amorphous materials is the so-called boson peak (BP).<sup>16</sup> It has been suggested that there is a direct correlation between TLS and the BP in glasses,<sup>17-19</sup> but the relationship between these two different spectroscopic features is still under investigation.

In this paper the puzzling behavior of the TLS Raman activity of glassy systems is reexamined with the systematic measurement of the low-frequency, low-temperature Raman spectra of a number of silicate glasses. Our spectroscopic measurements on a series of soda-lime-silica glasses with various amounts of CaO and BaO as well as on a Steuben (PbO) glass show TLS Raman activity in each case. The precision of these measurements is sufficient to estimate the total Raman-active number density of TLS. It is found that this number density does not scale with the boson peak strength in the vibrational spectrum.

The next section outlines the theoretical background for the analysis of the temperature-dependent Raman scattering properties of glasses at low temperatures and low frequencies. Section III presents the experimental details and results. The data analysis is described in some detail in Sec. IV which permits an estimate of the total Raman-active number density of TLS to be made. The discussion and conclusions in Sec. V complete the picture.

**II. THEORETICAL BACKGROUND**

Raman spectroscopy is an important tool in the study of the vibrational properties of solids.<sup>20-22</sup> In glasses, most of the work has centered on the boson peak, a near-universal feature.<sup>19,23-26</sup> The experimental work to be presented and analyzed here focuses on the quasielastic scattering region of glasses and its temperature dependence, at somewhat lower frequencies ( $<25$  cm<sup>-1</sup>) and lower temperatures ( $<15$  K) than most of the earlier studies. At such low temperatures, relaxational Raman scattering effects can be neglected. Still the total Raman Stokes intensity has two temperature-

dependent contributions: the resonant interaction with TLS and with phonons, giving<sup>2</sup>

$$I_{\text{Total}}^S(\omega, T) = I_{\text{ph}}^S(\omega, T) + I_{\text{TLS}}^S(\omega, T), \quad (1)$$

where<sup>27</sup>

$$I_{\text{ph}}^S(\omega, T) = [n + 1] \left[ g_{\text{ph}}(\omega) \frac{C_{\text{ph}}}{\omega} \right] \quad (2)$$

and

$$I_{\text{TLS}}^S(\omega, T) = [n_{\text{TLS}}^S(\omega, T)] \left[ g_{\text{TLS}}(\omega) \frac{C_{\text{TLS}}}{\omega} \right]. \quad (3)$$

Here  $n_{\text{TLS}}^S$  is the ground-state population factor of TLS. It represents the fraction of TLS in the ground state at a given frequency and a given temperature, and it follows the Boltzmann distribution as  $n_{\text{TLS}}^S = 1/[1 + \exp(-\hbar\omega)/k_B T]$ . The density of states for phonons and TLS are  $g_{\text{ph}}(\omega)$  and  $g_{\text{TLS}}(\omega)$ , respectively.

To obtain an expression that brings out the temperature-dependent Raman scattering due to TLS, both sides of Eq. (1) are divided by the Bose-Einstein factor  $(n + 1)$  so that

$$\frac{I_{\text{Total}}^S(\omega, T)}{(n + 1)} = \left[ g_{\text{ph}}(\omega) \frac{C_{\text{ph}}}{\omega} \right] + \left[ g_{\text{TLS}}(\omega) \frac{C_{\text{TLS}}}{\omega} \right] \tanh \left[ \frac{\hbar\omega}{2k_B T} \right]. \quad (4)$$

It is interesting to note that the ratio of  $n_{\text{TLS}}^S/(n + 1)$  gives the tanh function above. By plotting this normalized Raman intensity data versus  $\tanh[\hbar\omega/2k_B T]$  the physical parameters of interest can be readily identified. If part of the low-frequency Raman scattering in glasses is due to TLS, then  $I_{\text{Total}}^S(\omega, T)/(n + 1)$  should depend linearly on  $\tanh[\hbar\omega/2k_B T]$ . Furthermore, the intercepts for such data sets give the phonon contribution and the slopes the TLS contribution to the total Stokes Raman intensity. With  $I_{\text{ph}}^S(\omega, T)$  known, the contributions from the TLS and the phonons on the anti-Stokes side can also be separated. The TLS contribution  $I_{\text{TLS}}^A(\omega, T)$  to the total anti-Stokes Raman intensity becomes

$$\begin{aligned} I_{\text{TLS}}^A(\omega, T) &= I_{\text{Total}}^A(\omega, T) - I_{\text{ph}}^A(\omega, T) \\ &= I_{\text{Total}}^A(\omega, T) - I_{\text{ph}}^S(\omega, T) \exp\left(\frac{-\hbar\omega}{k_B T}\right). \end{aligned} \quad (5)$$

Once the Raman scattering due to phonons is removed from the total Raman intensity, the Raman scattering due to TLS from both Stokes and anti-Stokes scattering contributions can be written as

$$I_{\text{TLS}}^j(\omega, T) = [n_{\text{TLS}}^j(\omega, T)] \left[ g_{\text{TLS}}(\omega) \frac{C_{\text{TLS}}}{\omega} \right], \quad (6)$$

where  $j=S$  or  $A$  stands for Stokes or anti-Stokes, respectively. Since the only temperature-dependent quantity on the right-hand side of Eq. (6) is the TLS population numbers  $n_{\text{TLS}}^j$ , plotting the Stokes intensity data versus the ground-state population number  $n_{\text{TLS}}^S$  or the anti-Stokes versus the

TABLE I. Sample ID, chemical composition, and density of the glasses studied.

Sample ID	Chemical composition	Density (g/cm <sup>3</sup> )
ALW <sup>a</sup>	12% CaO and 0% BaO	2.5
ALX <sup>a</sup>	9% CaO and 3% BaO	2.6
ALY <sup>a</sup>	6% CaO and 6% BaO	2.7
ALZ <sup>a</sup>	3% CaO and 9% BaO	2.8
AMA <sup>a</sup>	0% CaO and 12% BaO	2.9
PbO <sup>b</sup>	55% SiO <sub>2</sub> and 30% PbO	3.1

<sup>a</sup>Corning soda-lime-silica glasses—the other glass components are 73% SiO<sub>2</sub>, 14% Na<sub>2</sub>O, and 1% Al<sub>2</sub>O<sub>3</sub>.

<sup>b</sup>Corning Steuben (PbO) glass.

excited state population number  $n_{\text{TLS}}^A$  should result in linear dependences with the same slope, a characteristic feature of a TLS spectrum.

### III. EXPERIMENTAL DETAIL AND RESULTS

The different glasses used in this investigation were prepared by Corning Incorporated. The chemical composition and the densities are listed in Table I. All of the glass samples studied were in the form of 5-mm cubes which had been polished to optical quality to reduce Rayleigh scattering.

An Oxford Variox optical cryostat is used for low-temperature measurements. The samples can either be immersed in superfluid <sup>4</sup>He or cooled with <sup>4</sup>He gas. The temperatures are monitored by three temperature sensors: a commercially calibrated rhodium-iron thermocouple placed on the heat exchanger near the sample, a commercially calibrated Lakeshore silicon diode thermocouple mounted on the sample holder, and a 1000-Ω Allen Bradley resistor also mounted on the sample holder. The most accurate temperature sensor is the Si-diode sensor on the sample holder, and the other thermometers are used as double checks. An Oxford ITC503 temperature controller is used to fix the temperature of the heat exchanger at the desired temperatures.

The Raman spectra have been measured with a Dilor XY 211 Raman system using the 514.532-nm excitation line of an argon ion laser. Each spectrum at a resolution of 2.10 cm<sup>-1</sup> was typically taken in a 600-sec duration using 200 mW of laser power. The usual 90° scattering configuration was used to study both the polarized and depolarized spectra. Both Stokes and anti-Stokes spectra have been recorded at each temperature. Low-temperature readings were checked by comparing the temperature values obtained from the Stokes and anti-Stokes spectra with the sample thermometer reading. In addition, no change was observed in the thermometer readings with the laser on and off. Because of the high transparency of the samples, it is perhaps not surprising that no laser-induced thermal heating of the samples is observed in these experiments. Therefore to a very good approximation the temperature measured by the sample thermometer is the actual temperature of the scattering volume even at low temperatures. In each case several spectra have been averaged to eliminate the effects of cosmic rays and other noise factors. To check for thermal hysteresis the tem-

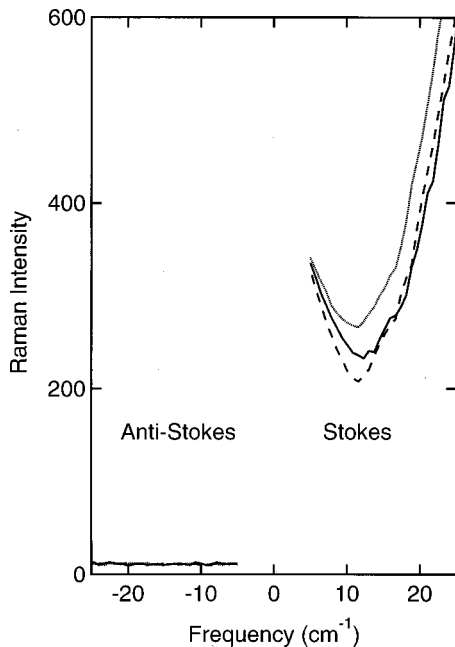


FIG. 1. Low-frequency polarized Raman spectra of some soda-lime-silica glasses covering both Stokes and anti-Stokes region at 1.4 K. The resolution is  $2.1 \text{ cm}^{-1}$ .

perature dependence of each sample is repeated twice: once with increasing temperatures and then with decreasing temperatures.

Low-temperature and low-frequency Raman spectra  $I_{\text{Total}}(\omega, T)$  are presented here either in this form, as described in the preceding section, or modified to  $I_{\text{Total}}(\omega, T)/\omega(n+1)$ . This latter frequency-weighted reduced spectrum<sup>28</sup> (FWRS) is convenient for displaying both the TLS scattering component (if any) and the vibrational contribution in the region of the boson peak. It also makes the presentation of our data consistent with previous work.<sup>2</sup>

#### A. Data for a series of soda-lime-silica glasses

The low-temperature polarized Raman spectra of a series of soda-lime-silica glasses with various amounts of CaO and BaO but with fixed total ionic concentration are shown in Fig. 1. On the Stokes side, there is strong Raman scattering even at 1.4 K. However, on the anti-Stokes side no Raman signal is observed at 1.4 K for any of the three glasses. To ensure that the elastic Rayleigh scattering does not influence the Raman spectra of these glasses, a lower limit of  $5 \text{ cm}^{-1}$  is used and as a result asymmetric spectra are obtained for the Stokes and anti-Stokes region at low frequencies. These asymmetric spectra indicate that Rayleigh scattering plays no significant role in our measurements, because such elastic scattering should enter into both the Stokes and anti-Stokes spectra with equal strength. Another reason for showing the anti-Stokes spectra is to demonstrate that there is no background signal due to luminescence. None is observed in our measurements.

The low-temperature FWRS (polarized and depolarized) of a series of soda-lime-silica glasses are shown in Fig. 2. The low-temperature spectra are all very similar. For the boson peak there is a slight shift to lower frequencies with

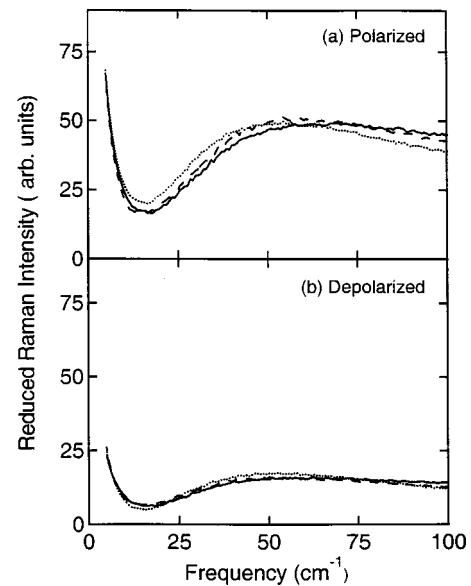


FIG. 2. Reduced Raman spectra of some soda-lime-silica glasses covering both the TLS and boson peak region at 1.4 K. (a) Polarized spectra, (b) depolarized spectra. Solid curve: (0.12CaO+0.0BaO) (ALW). Dashed curve: (0.06CaO+0.06BaO) (ALY). Dotted curve: (0.0CaO+0.12BaO) (AMA). The resolution is  $2.1 \text{ cm}^{-1}$ .

increasing BaO content. This frequency shift may be correlated with the change in glass density: the higher the density, the lower the frequency. For the lowest frequencies shown in the figure the scattering in each system increases dramatically. In addition, the strength of this low-frequency contribution in each of the glasses is essentially the same, independent of the glass density. Because of this similarity between the spectra of this glass series listed in Table I, the detailed temperature-dependent results for only one chemical composition are presented here.

The FWRS for the (6% CaO and 6% BaO) ALY soda-lime-silica glass at several temperatures are shown in Fig. 3. Figure 3(a) presents the polarized Raman intensity of the quasielastic scattering from  $5\text{--}15 \text{ cm}^{-1}$  from this ALY glass which increases with decreasing temperature from 12.5 K down to 1.4 K. Similar behavior is found in Fig. 3(b) for the depolarized spectra, but the scattering effect is noticeably weaker in this case. As will be shown in the next section, the experimental results for all of these soda-lime-silica glasses below 15 K display the predicted characteristic temperature-dependent behavior of Raman scattering due to resonant interaction with TLS.<sup>2</sup>

#### B. Data for PbO silicate glass

Mainly because previous workers reported no Raman scattering from TLS in a silicate lead glass,<sup>15</sup> some care has been taken to measure the low-temperature polarized and depolarized FWRS of a Stueben silicate glass containing a high concentration of PbO. The FWRS at several temperatures are shown in Fig. 4. The boson peak scattering shown in Fig. 4(a) is more than twice as strong as that from the (6% CaO and 6% BaO) ALY soda-lime-silica glass presented in

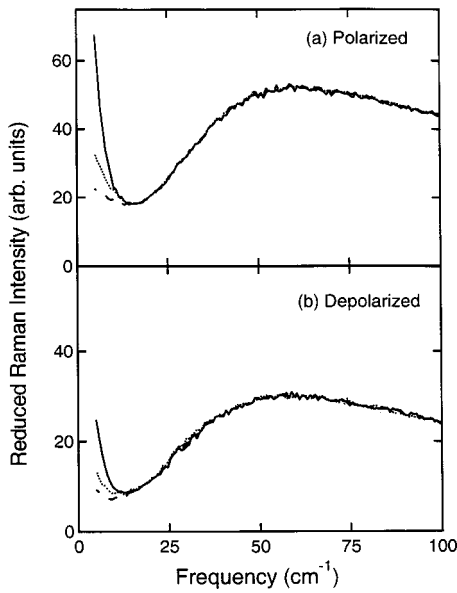


FIG. 3. Temperature dependence of the reduced Raman spectra of (0.06CaO+0.06BaO) soda-lime-silica glass. Solid curve: 1.4 K. Dotted curve: 7.5 K. Dashed curve: 12.5 K. (a) Polarized spectra, (b) depolarized spectra.

Fig. 3. No temperature dependence is observed in the boson peak region for these spectra; however, the polarized Raman intensity of the quasielastic scattering from 5 to 15  $\text{cm}^{-1}$  in this PbO glass is observed to increase with decreasing temperature from 12.5 K down to 1.4 K. This is the same characteristic temperature dependence found for the soda-lime-silica glasses indicating that Raman scattering from TLS is being observed. Note that the TLS effect is much weaker in this PbO glass as compared to the soda-lime-silica glasses despite the fact that the PbO glass is a

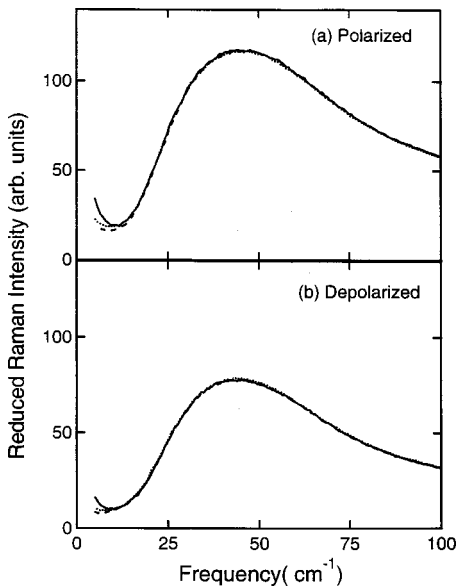


FIG. 4. Temperature dependence of the reduced Raman spectra of a PbO Steuben silicate glass. Solid curve: 1.4 K. Dotted curve: 7.5 K. Dashed curve: 12.5 K. (a) Polarized spectra, (b) depolarized spectra. The resolution is  $2.1 \text{ cm}^{-1}$ .

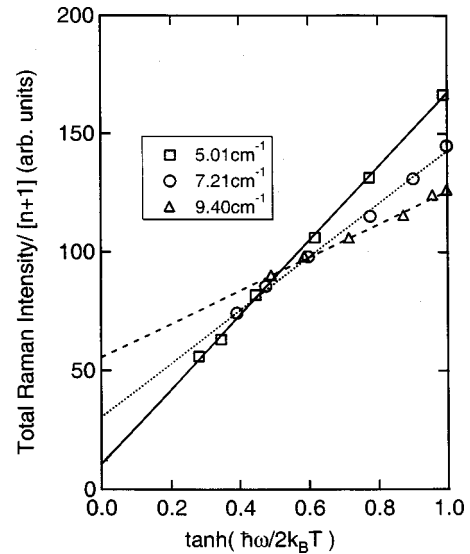


FIG. 5. Population dependence of the total Stokes Raman scattering normalized by  $(n+1)$ . For a (0.06CaO+0.06BaO) soda-lime-silica glass a linear variation vs  $\tanh[\hbar\omega/2k_B T]$  is shown for three different frequencies in the quasielastic region and six temperatures from 1.4 to 15 K.

more efficient Raman scatterer. (Compare the boson peak region, for example.) Similar temperature-dependent behavior is observed in Fig. 4(b) for the depolarized spectra. Clearly, Raman scattering from resonant interaction with TLS results occurs for this PbO glass, consistent with the soda-lime-silica results and contradicting the results previously reported for a PbO silicate glass.<sup>15</sup>

#### IV. DATA ANALYSIS

##### A. Detailed TLS temperature dependence of some silicate glasses

To provide a quantitative determination of the temperature-dependent results it is necessary to make use of Eq. (4) to analyze the data. In Fig. 5, the appropriately normalized low-frequency Raman spectra  $I_{\text{Total}}^S(\omega, T)/(n+1)$  is plotted versus  $\tanh[\hbar\omega/2k_B T]$  from 1.4 to 15 K for the soda-lime-silica glass (6% CaO and 6% BaO) ALY. The linear dependence over the six temperatures and three frequencies (with no free parameters) clearly demonstrates that Raman scattering from TLS is being observed for this soda-lime-silica glass.

After removing the phonon contribution from the total Raman intensity, the observed linear dependence of the Raman TLS scattering data versus the population of the appropriate Stokes or anti-Stokes scattering state is presented in Fig. 6. The Raman Stokes intensity without the phonon contribution versus  $n_{\text{TLS}}^S$  is plotted in Fig. 6(a) for the soda-lime-silica glass. Clearly, the Raman Stokes intensity depends linearly on the ground state  $n_{\text{TLS}}^S$  for the three frequencies shown. Because both the temperatures and frequencies are determined, the slope in Eq. (6) is the experimentally measured quantity of interest. Similar behavior is observed on

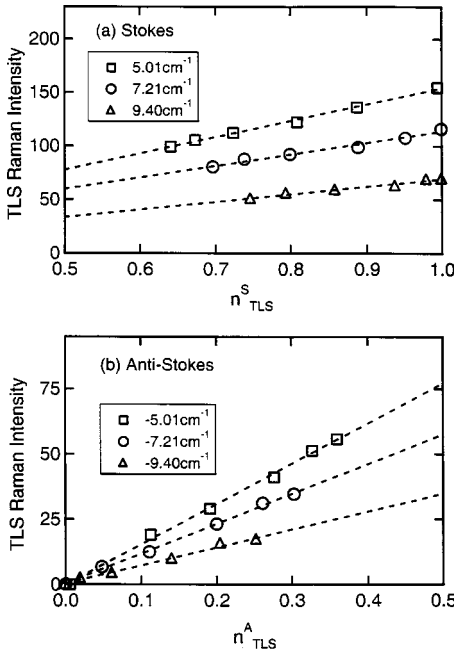


FIG. 6. Temperature dependence of low-frequency Raman intensity due to TLS, for a (0.06CaO+0.06BaO) (ALY) soda-lime-silica glass from 1.4 to 15 K. (a) Raman Stokes intensity vs the ground-state population,  $n^S_{\text{TLS}}$ , (b) Raman anti-Stokes intensity vs the excited state population,  $n^A_{\text{TLS}}$ .

the anti-Stokes side, as shown in Fig. 6(b). Within experimental error the same slope is found.

The same linear dependence is observed for all the soda-lime-silica glasses listed in Table I. Raman spectroscopy has the added advantage that both Stokes and anti-Stokes scattering can be examined separately so that there is no free parameter involved in fitting the experimental data to Eq. (6) when both the Stokes and anti-Stokes data are used. Similar behavior is seen in the depolarized spectra, but clearly the effect is much weaker. The Raman scattering contribution from resonant interaction with TLS has been determined for all of these soda-lime-silica glasses and will be presented shortly.

The same procedure described for the soda-lime-silica glasses has also been used to analyze the PbO glass results. The observed linear dependence of the Raman TLS scattering versus population of the appropriate scattering state is shown in Fig. 7 for the Steuben PbO glass. Clearly, the Raman Stokes intensity without the phonon component depends linearly on  $n^S_{\text{TLS}}$  for the three frequencies shown in Fig. 7(a). Similar behavior is observed on the anti-Stokes side shown in Fig. 7(b) with the same slope and for the depolarized spectra. Even though the observed Raman scattering from TLS in this PbO glass is much weaker compared to the soda-lime-silica glass, the signal to noise was sufficient to demonstrate the TLS temperature effect. It appears that previous investigators missed seeing this effect in the PbO glass<sup>15</sup> because the TLS scattering does not scale with the scattering associated with the vibrational modes.

### B. Density of states of TLS in silicate glasses

To obtain a measure of the density of states per unit volume,  $g_{\text{TLS}}(\omega)$ , of Raman-active TLS for silicate glasses, the

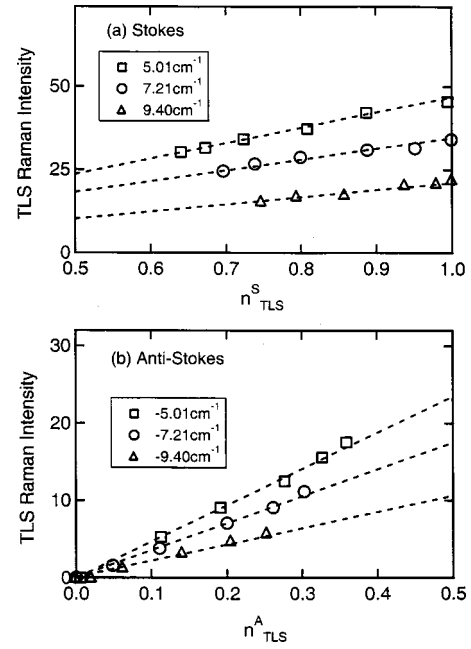


FIG. 7. Temperature dependence of low-frequency Raman intensity due to TLS, for a Steuben PbO glass from 1.4 to 15 K. (a) Raman Stokes intensity vs the ground-state population,  $n^S_{\text{TLS}}$ , (b) Raman anti-Stokes intensity vs the excited state population,  $n^A_{\text{TLS}}$ .

Raman intensity due to TLS must be normalized to that of a Raman band with a known density of states. The Raman scattering from vibrational modes in pure fused  $\text{SiO}_2$  has been examined.<sup>16</sup> The predominant feature in pure fused  $\text{SiO}_2$  is the strong and polarized double-peaked band centered at  $400 \text{ cm}^{-1}$ . Although part of this spectrum probably arises from the motion of bridging oxygen along the Si-O-Si angle bisector, which is often described as the symmetric stretching mode of bridge oxygen,  $\nu_s(\text{Si-O-Si})$ ,<sup>29</sup> this is still controversial. We therefore propose here to use a more general argument to determine the appropriate normalizing density of states.

The high-temperature specific heat in the Dulong-Petit limit can be interpreted in terms of nine normal modes per  $\text{SiO}_2$  molecule, three translational vibrations, three librational vibrations, and three internal vibrations. The experimental specific heat result at high temperatures together with the vibrational density of states measured by inelastic neutron scattering<sup>30</sup> can be used to estimate the mean number of modes in the Raman-active frequency band of interest. The full width at half maximum (FWHM) of this band ranges from  $250$  to  $510 \text{ cm}^{-1}$ . From the experimentally measured density of states this frequency range encompasses on the average three modes per molecule. Assuming that about  $1/2$  of these modes are Raman active, the normalizing factor for the scattered intensity in this frequency region becomes  $S_M \sim 3.3 \times 10^{22} \text{ mode/cm}^3$ .

An estimate of the total density of states of TLS per unit volume,  $g_{\text{TLS}}(\omega)$ , can be obtained from the Raman scattering results by comparing the ratio between the polarized Raman scattering found for TLS with that found for the polarized band from  $250$  to  $510 \text{ cm}^{-1}$  in pure fused  $\text{SiO}_2$ . Because both the symmetric and asymmetric contributions

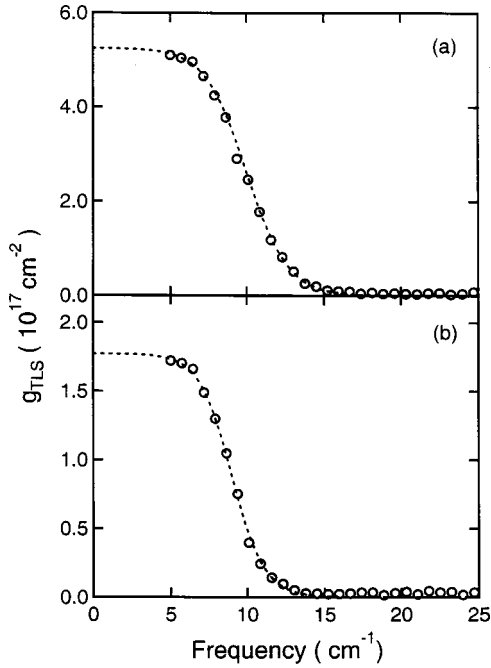


FIG. 8. Frequency dependence of the optical number density of states of TLS, in two silicate glasses at 1.4 K. (a) (0.06CaO + 0.06BaO) soda-lime-silica glass, (b) Steuben PbO silicate glass.

are included in the polarized spectrum, this comparison gives a measure of the total density of states of TLS. If  $C_M$  is taken to be the light-vibration coupling coefficient for these high-frequency Raman-active vibrational modes, then a zero-order approximation is to assume that the TLS coupling coefficient  $C_{\text{TLS}} \sim C_M = \text{const}$ . One gets the following equation:

$$\frac{\omega(I_{\text{TLS}}^S/n_{\text{TLS}}^S)}{\int d\omega \omega I_M^S} = \frac{g_{\text{TLS}}(\omega)}{\int d\omega g_M(\omega)} = \frac{g_{\text{TLS}}(\omega)}{S_M}, \quad (7)$$

where  $I_{\text{TLS}}^S$  is the Raman Stokes intensity from TLS and  $I_M^S$  is the Raman Stokes intensity from the high-frequency phonon band. The numerator of Eq. (7) on the left-hand side is the left-hand side of Eq. (3) divided by  $C_{\text{TLS}}n_{\text{TLS}}^S/\omega$  and the denominator is the left-hand side of Eq. (2) divided by  $C_M(n_M+1)/\omega$  integrated over the region from 250 to 510 cm<sup>-1</sup>. Note that the Bose-Einstein factor for the high-frequency vibrational mode,  $(n_M+1)$ , has been set to unity in Eq. (7) because the sample is at 1.4 K. Since the experimental ratio on the left-hand side is known for each sample and so is  $S_M$ , the mean number of Raman-active vibrational modes per unit volume, the value of  $g_{\text{TLS}}(\omega)$  can be determined explicitly:

$$g_{\text{TLS}}(\omega) = S_M \frac{\omega(I_{\text{TLS}}^S/n_{\text{TLS}}^S)}{\int d\omega \omega(I_M^S)}. \quad (8)$$

In Fig. 8(a), the density of states per unit volume of TLS,  $g_{\text{TLS}}(\omega)$ , is plotted versus frequency for the ALY soda-lime-silica glass. Note that the high-frequency cutoff for TLS in this glass is  $\sim 15.0$  cm<sup>-1</sup>. Similar behavior is found for each of the other soda-lime-silica glasses as illustrated in Fig. 1. Figure 8(b) shows the density of states per unit volume for

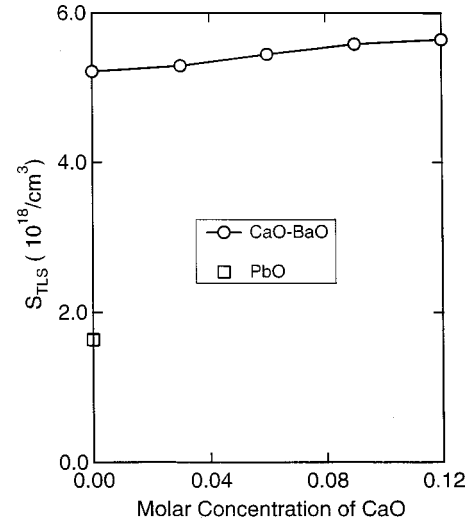


FIG. 9. Comparison of the total optical number density of Raman-active TLS,  $S_{\text{TLS}}$ , for several different glasses. The soda-lime-silica glasses are shown vs the CaO concentration.

the PbO glass. Here the high-frequency cutoff appears slightly lower with a cutoff at  $\sim 14.0$  cm<sup>-1</sup>. Since the optical density of states is being measured, the cutoff either signifies a change in the TLS Raman activity or the density of states goes to zero. Since optical selection rules for tunneling systems are known to change when the asymmetry becomes comparable with the symmetric tunnel splitting, these measurements suggest that a crossover may extend up to an energy of about 1 meV. Clearly the assumption often used to analyze low-temperature thermal data that the density of states of TLS is a constant<sup>8</sup> would still be valid in this case.

### C. Total number density of TLS

The existence of the high-frequency cutoff in the TLS optical density of states,  $g_{\text{TLS}}(\omega)$ , for these glasses permits an estimation of the total number of Raman-active TLS per unit volume,  $S_{\text{TLS}}$ . Each of the dotted curves displayed in Figs. 7(a) and 7(b) represents a least-squares fit to  $g_{\text{TLS}}(\omega)$  using an empirical three-parameter function of the form  $g(\omega) = a/\{\exp[b(\omega-d)]+1\}$ , where  $a$ ,  $b$ , and  $d$  are the fitting parameters. Since the fits are extremely good, the fitted function  $g_{\text{TLS}}(\omega)$  is used to estimate the area under each curve. Integrating

$$\int d\omega g_{\text{TLS}}(\omega) = S_{\text{TLS}}, \quad (9)$$

from 0 to 100 cm<sup>-1</sup> gives the total number of Raman-active TLS per unit volume,  $S_{\text{TLS}}$ .

For the soda-lime-silica glass series the measured total number density of Raman-active TLS,  $S_{\text{TLS}}$ , at 1.4 K is presented in Fig. 9 as a function of the molar concentration of CaO. Note that  $S_{\text{TLS}}$  increases only slightly as the CaO content increases. The data point corresponding to the PbO

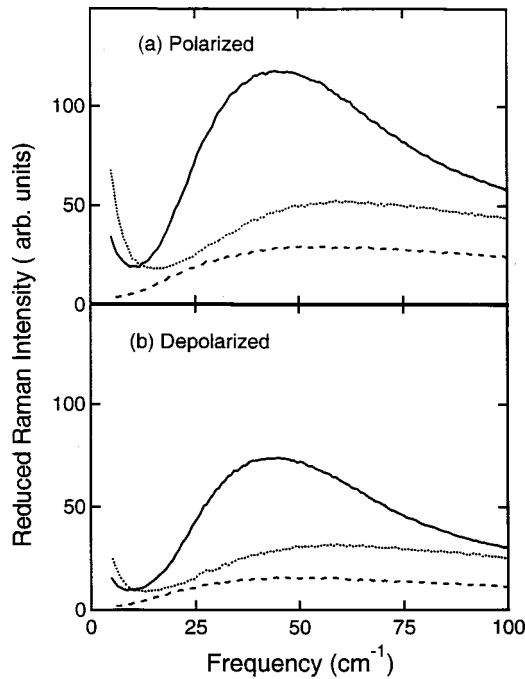


FIG. 10. Comparison of the low-frequency reduced Raman spectra of several different glasses at 1.4 K. Dashed curve: fused  $\text{SiO}_2$ . Dotted curve: (0.06CaO+0.06BaO) soda-lime-silica glass. Solid curve: Steuben PbO silicate glass. (a) Polarized spectra, (b) depolarized spectra. Note that the largest boson peak scattering does not correlate with the largest TLS scattering.

glass is also included for reference. For the PbO glass,  $S_{\text{TLS}}$  is about a factor of 3 smaller than that found for the soda-lime-silica glasses.

#### D. No scaling of TLS with the boson peak

Low-frequency FWRS of several representative glasses at 1.4 K are shown in Fig. 10. Both polarized and depolarized spectra are presented in (a) and (b), respectively. Raman scattering from TLS is most intense for the soda-lime-silica glass ALY (dotted curve), weaker in the PbO glass (solid curve) and not observed in fused  $\text{SiO}_2$  glass (dashed curve).

An important experimental find illustrated here is that the scattering in the boson peak region does not scale in the same way as the scattering from TLS: the boson peak (vibrational scattering) is strongest in the PbO glass, weaker in the ALY glass and the weakest in the fused  $\text{SiO}_2$  glass. The TLS scattering, on the other hand, is strongest for the ALY glass, weaker for the PbO glass and absent in the pure  $\text{SiO}_2$  glass as determined in Ref. 5. The conclusion is that in glasses the intensity of the Raman scattering from TLS and scattering in the boson peak region do not scale with one another.

#### E. No Raman scattering from TLS excited-state transitions

Previous far-infrared low-temperature studies<sup>10,31</sup> of both fluorite mixed crystals and glasses have shown that there are TLS excited-state transitions in the region from  $\sim 20$  to  $40 \text{ cm}^{-1}$ . These excited-state excitations manifest themselves by

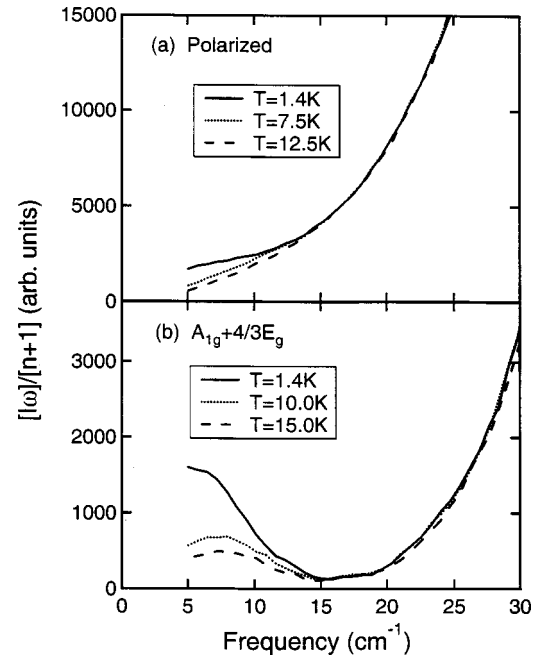


FIG. 11. Temperature dependence of the low-frequency reduced Raman spectra of two different kinds of disordered systems. (a) (0.06CaO+0.06BaO) soda-lime-silica glass (ALY). Solid curve: 1.4 K. Dotted curve: 7.5 K. Dashed curve: 12.5 K. (b)  $(\text{BaF}_2)_{0.55}(\text{LaF}_3)_{0.45}$  fluorite mixed crystal. Solid curve: 1.4 K. Dotted curve: 10.5 K. Dashed curve: 15.0 K.

having the opposite temperature dependence at low temperatures, over a restricted frequency interval, from that found for the ground-state TLS transitions. At low temperatures as the TLS IR-active spectrum disappears with increasing temperature, the excited-state IR-active spectrum appears.

Figure 11 shows the temperature-dependent Raman spectra for a soda-lime-silica glass and for a fluorite mixed crystal now plotted in such a way as to bring out any Raman-active excited-state population effects if they exist. In Fig. 11(a),  $\omega I_{\text{Total}}(\omega, T)/(n+1)$  for a soda-lime-silica glass (6% CaO and 6% BaO) ALY is shown for several temperatures. This combination gives an ordinate proportional to the density of states times the coupling coefficient. At low frequencies the TLS temperature dependence is evident. However, in the frequency region  $20\text{--}40 \text{ cm}^{-1}$  (as well as the entire boson peak region, not shown) no change is observed in the spectrum for different temperatures. This result is completely different from the far-infrared results which display IR-active TLS excited-state transitions.<sup>10</sup> Such a constant result with temperature would be expected if the low-temperature Raman scattering in this frequency region is only associated with phonons. Since there is no additional temperature dependence, it appears that the TLS excited states in this soda-lime-silica glass (and the PbO glass) are not Raman active.

The  $\text{BaF}_2 + 45\% \text{LaF}_3$  mixed crystal Raman scattering data, which are shown in Fig. 11(b) for a similar temperature range, further demonstrate the absence of Raman-active TLS excited-state transitions. Here any TLS excited-state temperature dependence would be easy to identify since the bo-

son peak is relatively weak, yet there is not the slightest evidence in this figure for Raman-active TLS excited-state transitions.

## V. CONCLUSIONS

By examining the Raman scattering from TLS in glasses a number of new features have been identified. The shift of the boson peak to lower frequencies with increased BaO concentration and the absence of such a shift for the corresponding TLS spectrum in the soda-lime-silica glasses shown in Fig. 1 are the first bit of direct evidence that the two components are not connected to each other. The fact that the PbO silicate glass has a much stronger boson peak but a much weaker TLS component when compared to the soda-lime-silica glasses reinforces this conclusion. The cutoff in the Raman activity of TLS for all of these glasses is consistent with symmetric tunnel splittings extending up to an energy of about 1 meV. This value provides a general lower limit for the barrier heights and/or the masses of the tunneling objects.

Explaining such detailed experimental results becomes even more challenging when it is realized that many features are very similar or identical to those previously reported for the Raman scattering from TLS in mixed fluorite crystal systems.<sup>13</sup> For both mixed crystal and glass systems, the optical density of states and total number density of Raman-

active TLS are similar in magnitude with the Raman cutoff frequency always occurring between 10 and 20 cm<sup>-1</sup>, moreover, in neither kind of disordered system is scaling of the strength of the TLS with the strength of the boson peak found.

No evidence of excited-state transitions associated with TLS have been observed in Raman scattering from the glasses or the mixed crystal systems, although both kinds of systems show TLS excited-state transitions in far-infrared absorption measurements. How such low-symmetry tunneling systems could still have a remaining selection rule is not at all clear.

One noteworthy difference in the TLS Raman scattering between the mixed crystal and glasses is that for the mixed crystal the TLS scattering only appears in  $A_{1g}$  symmetry, not in  $E_g$  or in  $T_{2g}$ . If the Raman scattering from the TLS in glasses were exactly the same, then scattering would have appeared only in the polarized spectrum not in the depolarized one. Such behavior was not observed.

## ACKNOWLEDGMENTS

We thank D. M. Trotter and M. Teter for providing us with the glass samples used in this study. This work was supported in part by NSF-DMR, NASA, and the CCMR facilities at Cornell University.

- 
- <sup>1</sup>G. Winterling, Phys. Rev. B **12**, 2432 (1975).  
<sup>2</sup>N. Theodorakopoulos and J. Jäckle, Phys. Rev. B **14**, 2637 (1976).  
<sup>3</sup>K. K. Mon, Y. C. Chabal, and A. J. Sievers, Phys. Rev. Lett. **35**, 1352 (1975).  
<sup>4</sup>M. A. Bösch, Phys. Rev. Lett. **40**, 879 (1978).  
<sup>5</sup>R. H. Stolen and M. A. Bösch, Phys. Rev. Lett. **48**, 805 (1982).  
<sup>6</sup>K. B. Lyons, P. A. Fleury, R. H. Stolen, and M. A. Bösch, Phys. Rev. B **26**, 7123 (1982).  
<sup>7</sup>W. A. Phillips, in *Amorphous Solids*, edited by W. A. Phillips (Springer-Verlag, Berlin, 1981).  
<sup>8</sup>W. A. Phillips, Rep. Prog. Phys. **50**, 1657 (1987).  
<sup>9</sup>S. A. FitzGerald, J. A. Campbell, and A. J. Sievers, Phys. Rev. Lett. **73**, 3105 (1994).  
<sup>10</sup>S. A. FitzGerald, A. J. Sievers, and J. A. Campbell, J. Phys.: Condens. Matter **13**, 2177 (2001).  
<sup>11</sup>J. J. Tu, J. A. Campbell, and A. J. Sievers, Bull. Am. Phys. Soc. **41**, 549 (1996).  
<sup>12</sup>J. J. Tu, S. A. FitzGerald, J. A. Campbell, and A. J. Sievers, J. Non-Cryst. Solids **203**, 153 (1996).  
<sup>13</sup>J. J. Tu and A. J. Sievers, Phys. Rev. Lett. **83**, 4077 (1999).  
<sup>14</sup>J. L. Prat, F. Terki, and J. Pelous, Phys. Rev. Lett. **77**, 755 (1996).  
<sup>15</sup>F. Terki, J. L. Prat, and J. Pelous, Philos. Mag. B **77**, 373 (1998).  
<sup>16</sup>S. R. Elliott, *Physics of Amorphous Materials* (Wiley, New York 1990).  
<sup>17</sup>U. Buchenau, Y. M. Galperin, V. L. Gurevich, and H. R. Schober, Phys. Rev. B **43**, 5039 (1991).  
<sup>18</sup>A. P. Sokolov, E. Rössler, A. Kisliuk, and D. Quitman, Phys. Rev. Lett. **71**, 2062 (1993).  
<sup>19</sup>A. P. Sokolov, R. Calemczuk, B. Salce, A. Kisliuk, D. Quitmann, and E. Duval, Phys. Rev. Lett. **78**, 2405 (1997).  
<sup>20</sup>A. S. Barker and A. J. Sievers, Rev. Mod. Phys. **47**, Suppl. 2, FS1 (1975).  
<sup>21</sup>W. Hayes and R. Loudon, *Scattering of Light by Crystals* (Wiley, New York, 1978).  
<sup>22</sup>S. R. Elliott, Nature (London) **354**, 445 (1991).  
<sup>23</sup>J. Jäckle, in *Amorphous Solids*, edited by W. A. Phillips (Springer-Verlag, Berlin, 1981).  
<sup>24</sup>A. P. Sokolov, A. Kisliuk, M. Soltwisch, and D. Quitmann, Phys. Rev. Lett. **69**, 1540 (1992).  
<sup>25</sup>M. Kolesik, D. Tunega, and B. P. Sobolev, Solid State Ionics **58**, 237 (1992).  
<sup>26</sup>A. P. Sokolov, A. Kisliuk, D. Quitmann, and E. Duval, Phys. Rev. B **48**, 7692 (1993).  
<sup>27</sup>R. Shuker and R. W. Gammon, Phys. Rev. Lett. **25**, 222 (1970).  
<sup>28</sup>J. S. Lannin, Phys. Rev. B **15**, 3863 (1977).  
<sup>29</sup>S. K. Sharma, D. W. Matson, J. A. Philpotts, and T. L. Roush, J. Non-Cryst. Solids **68**, 99 (1984).  
<sup>30</sup>D. L. Price and J. M. Carpenter, J. Non-Cryst. Solids **92**, 153 (1987).  
<sup>31</sup>S. A. FitzGerald, A. J. Sievers, and J. A. Campbell, J. Phys.: Condens. Matter **13**, 2177 (2001).